Characterization of Neutron Reaction Rates in Different Irradiation Channels of the CNESTEN's TRIGA Mark II Research Reactor

Hamza Ghninou, Adrien Gruel, Abdallah Lyoussi, Christelle Reynard-Carette, Chafik El Younoussi, Bilal El Bakkari, Bouzekri Nacir, Yassine Boulaich, Hamid Bounouira

Characterization of Neutron Reaction Rates in Different Irradiation Channels of the CNESTEN's TRIGA Mark II Research Reactor

H. Ghninou[1], A. Gruel[1], A. Lyoussi[1], C. Reynard-Carette[2], C. El Younoussi[3], B. El Bakkari[3], B. Nacir[3], Y. Boulaich[3], H. Bounouira[3]

[1] CEA/DES/IRESNE/DER/SPESI, Cadarache, F-13108 Saint-Paul- lez-Durance, France
[2] Aix-Marseille University, Université de Toulon, CNRS, IM2NP, 13013 Marseille, France
[3] CNESTEN/CENM, Rabat 10001, Morocco

Abstract

The National Center for Energy, Sciences and Nuclear Techniques (CNESTEN)'s Training Research and Isotope Production General Atomics (TRIGA) Mark II is a pool-type light water moderated and cooled research reactor operating at a maximum steady state thermal power of 2 MW. The reactor was designed to be used as a training facility for reactor operators, neutron activation analysis, isotopes production, and for implementing different reactor physics experiments. This article deals with the numerical and experimental characterization of reaction rates (RRs) in different irradiation channels inside the CNESTEN's TRIGA Mark II research reactor, located in Rabat/Morocco. The main objective of this study is to validate the calculated neutron RRs against the measured ones and to prove that the new TRIPOLI-4 model of the reactor is capable to reproduce the measured quantities. Therefore, the measurements were carried out using the neutron activation technique and gamma spectrometry measurements. Preliminary simulations were performed with TRIPOLI-4 transport Monte Carlo code to establish the experimental design and set up for activation foils experiments. The selected set of foils with known characteristics were irradiated, at different power levels, inside the irradiation facilities of the TRIGA reactor. The resulting activities were evaluated via γ spectrometry measurements. Normalized calculated and measured RRs were compared, and a good agreement was shown for most nuclides, which indicates that the new detailed TRIPOLI-4 model of the TRIGA reactor can accurately predict the relative experimental RRs values. Further work is ongoing to analyze absolute RR values, as well as to carry measurements in other irradiation channels.

Keywords – Activation foils, in-core dosimetry, TRIPOLI-4 simulations, γ spectrometry.

1. Introduction

National Center for Energy, Sciences and Nuclear Techniques (CNESTEN) located in Rabat, Morocco, operates a 2-MW Training Research and Isotope Production General Atomics (TRIGA) Mark II research reactor. This reactor is equipped with several irradiation channels: in-core irradiation channels are designed for high neutron flux irradiations, whereas ex-core ones can provide neutron flux with different characteristics (magnitude and energy spectra). In support of operation, physicists have a particle transport (neutron, photon, and electrons) calculation tool to determine the main physical parameters, such as neutron and photon flux levels, kinetic parameters, power peaking factors, excess reactivity of the core, and control rods worth. These data are particularly useful during the design of new experiments, to check upstream compliance with the safety criteria.

In the past few years, a complete computational model of the TRIGA reactor was developed using the 3-D continuous energy Monte-Carlo N-Particle Transport Code (MCNP) [1] to support planning, design, and implementation of new experiments within and beyond the reactor core. Several studies were published using this computational model [2] – [5]. However, the experimental verification and validation of the computational model are now based on a limited number of experiments that have been carried out during the divergence phase of the reactor

[2]. For that specific reason, a collab- oration between the French Atomic Energy and Alternative Energies Commission (CEA) and the CNESTEN has been established to expand the utilization of the CNESTEN's TRIGA computational model by carrying out neutron activation measurements, allowing an advanced characterization of the irradiation facilities of the reactor. In addition, it was decided to develop a new detailed computational model of the TRIGA reactor using the 3-D Monte Carlo code TRIPOLI-4® [6]. This new calculation scheme will be dedicated to the preparation and analysis of experiments, such as neutron and gamma fields' characterization at various positions, innovative detector testing, and will be built to be able to carry easily uncertainty studies to provide reliable results.

The TRIPOLI-4 model was used to assess the experimental design through preliminary calculations to select dosimeters, which we can refer to as "activation foils" and to optimize the reactor power levels and the irradiation duration. This model was then used to calculate the reaction rates (RRs) of all targeted dosimeters to compare them with the measured ones. This article presents the results of the neutronic characterization of the irradiation channels of the CNESTEN's TRIGA Mark II research reactor. For this study, we shall start by providing a description of the reactor and the associated TRIPOLI-4 computational model. Then, we will delve into the two facets of the irradiations design, which are the experimental setup and the experimental design. After, we will present the irradiation of samples and spectrometry measurements. At last, the obtained results of this study are discussed.

2. Reactor description and TRIPOLI model

2.1. Reactor description

The Moroccan TRIGA Mark II is a research reactor designed and manufactured by General Atomics. It is a pool type light water cooled and moderated reactor using low-enriched uranium fuel that typically operates at a steady state thermal power up to 2 MW. The fuel material consists of a uniform mixture of uranium (8.5 wt%, enriched to 19.7% of ^{235}U), hydrogen, and zirconium. This composition leads to a large negative temperature reactivity coefficient, which makes the reactor inherently safe and suitable for training, nuclear research, radioisotopes production, and other utilizations. The reactor core is submerged in a light water pool of 2.5 m diameter and 8.8 m height. Fig. 1 presents the reactor core assembly, which is composed of 101 fuel elements (FEs), including 5 fuel-follower control rods (FFCRs), 17 graphite elements, a central thimble (CT), and a pneumatic transfer system (PTS). The latter can quickly transfer samples between the radiochemistry laboratory and the in-core irradiation position and is used to irradiate and transport specimens with short half-lives. The reactor is also equipped with a rotary specimen rack (RSR) containing 40 irradiation positions, which allows the irradiation of long half-lives specimens. In addition, the Moroccan TRIGA reactor is equipped with a thermal column and four beam channels penetrating the concrete shield, the aluminum tank, and the reactor tank. Beam port NB1 is a tangential port, whereas beam ports NB2 – 4 are radially oriented ports (see Fig. 1). These tubes allow beams of neutron and gamma radiation to pass from the reactor core to the outside of the reactor shield structure for experiments. The adjustment and control of the reactor power at steady state operation are achieved by five FFCRs, SHIM I–IV, and REGULATING, as shown in Fig. 1.

2.1. TRIPOLI modeling of TRIGA Mark II reactor

A new computational model of the CNESTEN's TRIGA reactor was developed using the 3-D continuous energy Monte Carlo code TRIPOLI-4.11 and the continuous energy cross sections from the JEFF3.1.1 nuclear data library. Figs. 1 and 2 provide radial and axial views of the reactor core model and show the main aspects of the model geometry. In this new model, the reactor core and all the irradiation facilities have been accurately modeled based on the manufacturer data.

After the development of the model geometry, it was used to perform neutron simulations, such as kinetic parameters, neutron flux levels, and power peaking distributions. The main objective

of these simulations is to verify the capability of the new TRIPOLI model to reproduce the results of the experiments that were realized during the divergence phase of the reactor. The results of TRIPOLI calculations were then compared with the experimental ones and to those obtained with the MCNP model. This comparison will be presented in a forthcoming paper.

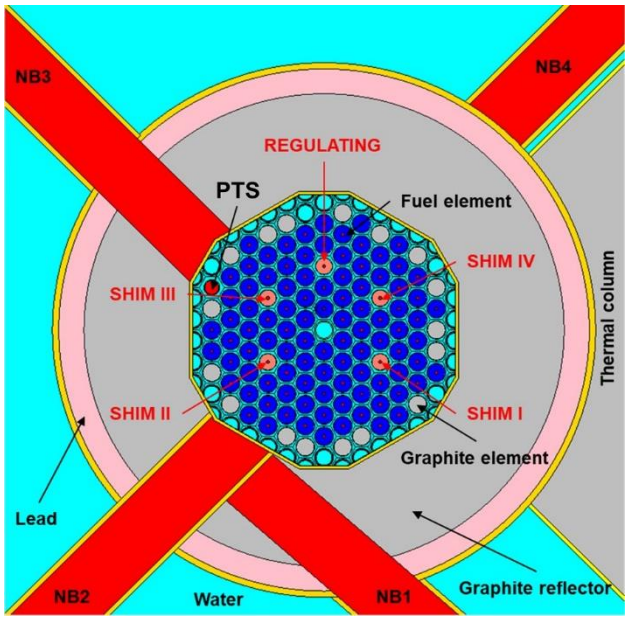

Fig. 1. Radial view of the TRIPOLI-4 model of the CNESTEN's TRIGAreactor in the current operating configuration.

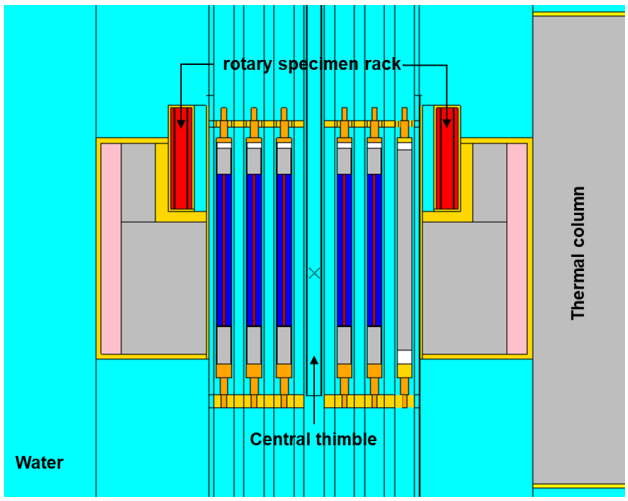

Fig. 2. Axial view of the TRIPOLI-4 model of the CNESTEN's TRIGA reactor in the current operating configuration.

3. Irradiation design

3.1. Experimental setup

As mentioned earlier, the CNESTEN's TRIGA reactor is composed of various irradiation facilities that are located within and beyond the reactor core. The main aim of this study is to characterize the RRs in different positions inside three irradiation facilities.

- CT: Characterization of different axial positions.
- PTS: Characterization of the irradiation position located in the outer ring at z =28 cm (regarding the mid-core plane, defined as the mid-fuel height).
- RSR: Characterization of eight irradiation channels among the 40 in this facility.

For each of these facilities, specific irradiation devices and specific specimen capsules were

used to ensure a reproducible positioning. Fig. 3 presents the irradiation device that was specifically designed to allow the positioning and the irradiation of the dosimeters within the CT.

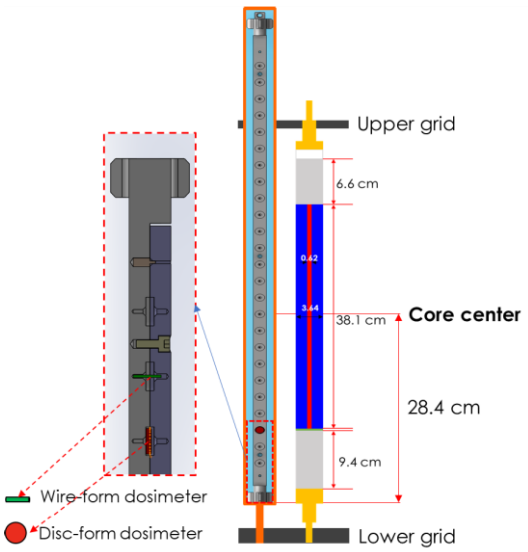

Fig. 3. Schematic of the experimental device that was used to position dosimeters in the CT irradiation facility.

For illustration purposes, neutron spectra were calculated at different irradiation positions and then normalized to 1 W (see Fig. 4).

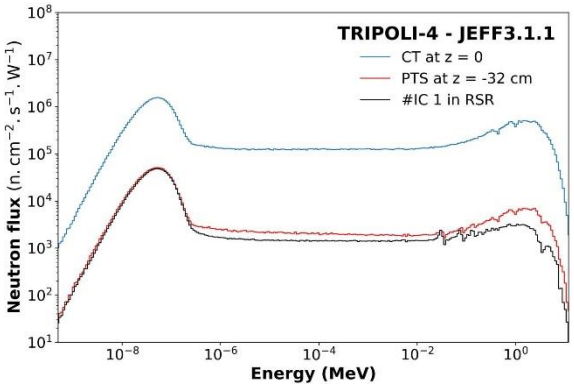

Fig. 4. Calculated neutron spectra (315 groups) in three irradiation facilities: the CT, the PTS, and the RSR, respectively.

In addition, the neutron flux within the irradiation channels of the RSR is presented in Fig. 5. The statistical uncertainty of neutron spectra calculations is around 0.1%–5%, whereas it is around 0.1%–0.2% for neutron flux calculations in the RSR facility.

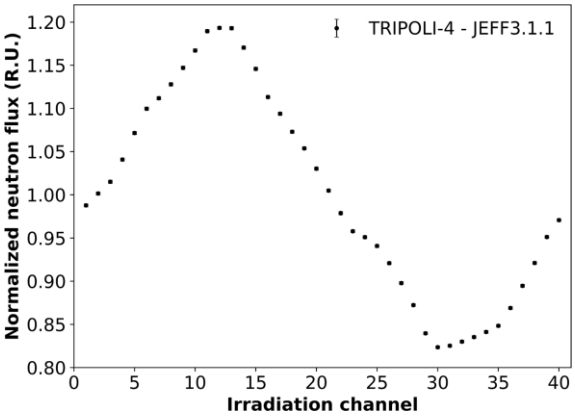

Fig. 5. Calculated normalized neutron flux in the 40 irradiation channels of the RSR.

The radial distribution of the thermal and total neutron flux, normalized to the maximum, is presented in Fig. 6(a) and (b). The latter shows that the total neutron flux is maximum at corecenter, which corresponds to 1.30×10^{14} n.cm^{-2}.s^{-1} when normalized to full power, 2 MW. The graphs also show that the total neutron flux decreases as it moves away from the center toward the peripheral rings of the reactor core. On the other hand, the radial distribution of the thermal neutron flux also shows a maximum at core center [see Fig. 6(a)], which is due to the presence of the CT, a water-filled channel, which leads to a high neutron moderation. One can also notice a slight increase in thermal flux in the water-filled spaces between FEs and in the graphite reflector elements that are positioned in the G ring.

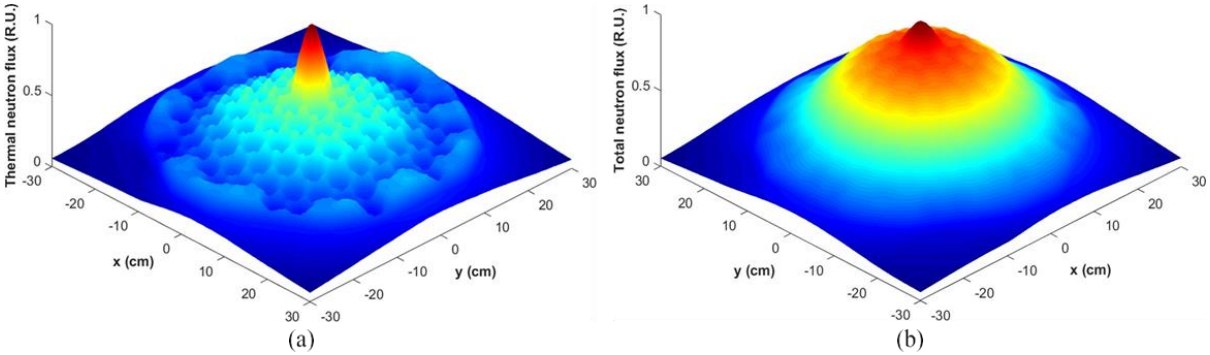

Fig. 6. (a) Radial distribution of thermal and (b) total neutron flux inside the core of the TRIGA reactor.

3.2. Experimental design

After the verification of the computational model, it was used to perform preliminary simulations to design the in-core activation dosimetry experiments. These simulations were performed to choose the dosimeters to be used to characterize the neutron flux and spectra, as well as to define the irradiations and gamma spectrometry measurement parameters. For that reason, we performed simulations to estimate the response of different dosimeters with known characteristics, and we selected those that can respond to a desired energy range of neutron spectra. Tables I and II present the characteristics, compositions, and dimensions of the dosimeters that were used to characterize the neutron flux inside the irradiation facilities of the CNESTEN's TRIGA reactor.

Dosimeter		**Reaction of interest**	**Half-life**	**Energy range of response**
Resonant	Gold	^{197}Au(n, γ)^{198}Au	2.6944 d	Th + epi
	Cobalt	^{59}Co(n, γ)^{60}Co	5.271 y	Th + epi
Threshold	Nickel	^{58}Ni(n, p)^{58}Co	70.82 d	E > 2.7 MeV
	Iron	^{56}Fe(n, p)^{56}Mn	2.578 h	E > 6.1MeV
	Titanium	^{46}Ti(n, p)^{46}Sc	83.787 d	E > 4.4 MeV
	Aluminum	^{27}Al(n, α)^{24}Na	14.957 h	E > 7.3 MeV

Table. I. Characteristics of the different isotopes [8] [9].

Composition	**Form**	**Diameter (mm)**	**Thickness (mm)**
Al – 0.1% Au	Disc	10	0.1
Al – 1% Co	Wire	1	10 (length)
99.98% Ni	Disc	10	0.125
99.99% Fe	Disc	10	0.125
99% Ti	Disc	10	0.5
99.999% Al	Disc	10	0.25

Table. II. Dosimeter's compositions and dimensions.

The selection criteria of these dosimeters are: the cross section of the neutron reaction of interest, the energy range of the response, the activation product half-life, and the energy and intensity of decay γ rays' emission. Thus, we simulated the response of the abovementioned dosimeters by calculating the RRs for each isotope at core center. Figs. 7 and 8 present the distribution of RRs and integrated RRs of the resonant and threshold dosimeters. From the integrated RRs, one can notice that resonant dosimeters show a large contribution of thermal neutrons due to the high value of the cross section in the thermal energetic domain of the (n, γ) reaction for both cobalt and gold dosimeters. Accordingly, the thickness of these dosimeters should be as small as possible to reduce the self- shielding effect. In our case, the dosimeters have a thickness of 0.1 mm for disk-form gold dosimeters and 1 mm diameter in the case of wire-form cobalt dosimeters. Furthermore, the threshold dosimeters, based on the threshold (n, p) and (n, α) reactions, are not sensitive to thermal neutron. As shown in Fig. 8, these dosimeters are only sensitive to fast neutrons above 1 MeV.

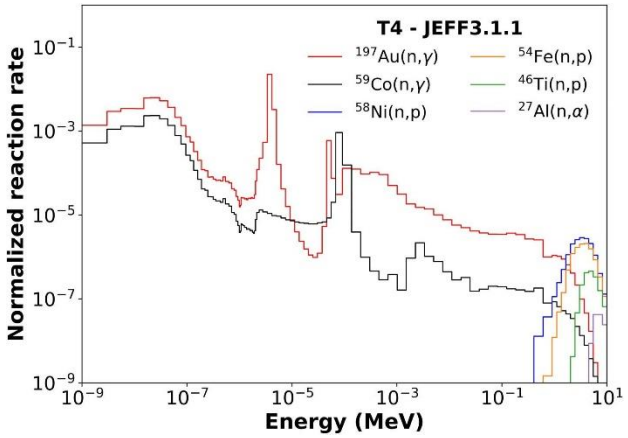

Fig. 7. Distribution of RRs for resonant and threshold dosimeters calculated with TRIPOLI.

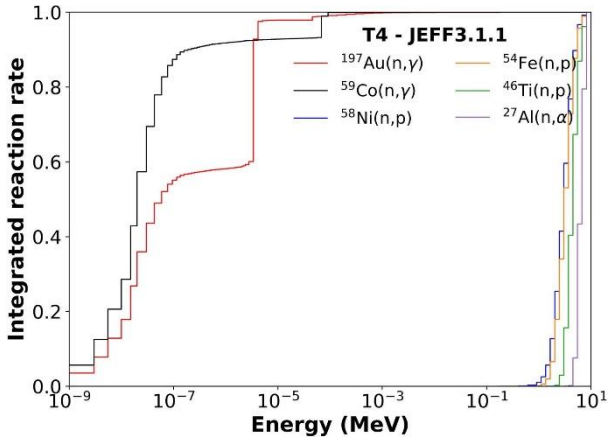

Fig. 8. Distribution of integrated RRs for resonant and threshold dosimeters.

After the selection of the dosimeters, RRs at different positions inside the three-irradiation channels were computed, by TRIPOLI-4 code, in order to estimate and optimize the mass and dimensions of the dosimeters, the irradiation duration and power level, as well as the spectrometry measurements duration. By scaling RRs scores to the power level using the scaling factor defined in (2), we can estimate the expected activities at the end of irradiation using the following formula:

$$A(t_i) = R_{T4} F_s \left(1 - e^{-\lambda t_i}\right) \quad (1)$$

where R_{T4} is the RR score calculated with TRIPOLI-4, t_i is the irradiation duration in s, λ is the decay constant in s^{-1}, and F_s, given in neutron.s^{-1}, is a scaling factor that was applied to normalize the RRs scores to a desired power level, and this factor is obtained by the following

formula [10]:

$$F_s = \frac{P\bar{\nu}}{w_f k_{eff}} \quad (2)$$

where P is the reactor power in W, $\bar{\nu}$ is the average number of prompt neutrons per fission, w_f is the energy released per fission (MeV/fission), and k_{eff} is the effective multiplication factor of the reactor.

Experimentally, the specific activity at the end of irradiation is given by the following formula [8]:

$$A_j = \frac{N(E_j)}{m I_\gamma(E_j) R^P(E_j) T(E_j) t_m} \prod_i C_i \quad (3)$$

where $N(E_j)$ is the number of counts in the absorption peak of energy E_j, m is the mass in g, of the dosimeter, $I_\gamma(E_j)$ is the intensity of the photon emission with energy E_j, $R^P(E_j)$ is the detector's efficiency for the photon with energy E_j, t_m is the measurement (counting) duration, in s, $T(E_j)$ is the yield transfer factor for the photon with energy E_j and C_i are the correction coefficients of dead-time, decay, coincidences. These factors are presented in details in IV-C.

By combining (1) and (3) and by taking the half-life of the irradiated samples and the detector's efficiency into account, we were able to define the irradiation, decay and measurement durations and the irradiation power level. Hence, in order to optimize these parameters; a number of counts under the total absorption peak greater than 10^4 has to be considered, leading to a statistical uncertainty of less than 1%.

In this preparation phase, a model of the CNESTEN's High Purity Germanium (HPGe) gamma detector was developed using the TRIPOLI-4.11 code. The detector's geometry and composition are based on the manufacturer data (cf. Fig. 9). In order to determine the detector's efficiency via TRIPOLI-4 simulations, we calculated the spectrum of activation photon deposited energy, pulse height distribution, in the detector. Simulations were run by generating 10^{10} mono-energetic photons emitted in an isotropic manner from a punctual source covering the energy range of 10 - 2000 keV (with 2000 energy bins). This model is used to evaluate the detector's efficiency, which was used to carry out the design of the experiments and to estimate the yield transfer factor that takes into account the difference in shape between the standard sources used for the detector efficiency evaluation and the measured samples (cf. IV.C).

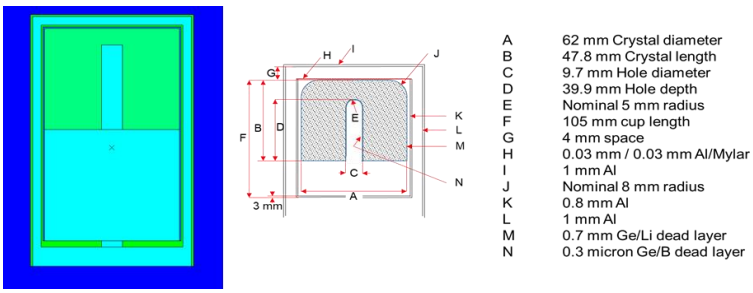

Fig. 1. TRIPOLI-4 model of the CNESTEN's HPGe detector.

4. Irradiations and spectrometry measurements

4.1. Samples irradiation and spectrometry measurements

The selected dosimeters (Tables I and II) were precisely cut, engraved, and weighed to allow an accurate RRs and neutron flux evaluation. Several irradiations were performed in the CNESTEN's TRIGA reactor between December 2020 and April 2021. The irradiation power level and duration were defined based on the preliminary simulations that were carried out

during the designing of experiments (see Table III).

At the end of irradiation, the analysis of the irradiated dosimeters is performed by means of the γ spectrometry technique using the CNESTEN's HPGe detector. Fig. 10 shows a measured gamma spectra of some dosimeters irradiated in the CT and the PTS. The count is given on a logarithmic scale to illustrate the significance of the peak energy. Peak areas are estimated with the sum algorithm of the GAMMA-VISION software. In addition, the marked peaks in Fig. 10 represent the main gamma peaks of the irradiated dosimeters. However, the unmarked peaks are mainly due to the impurities in the dosimeter composition. After the acquisition, the activity of an irradiated sample can be obtained using (3).

Date of irradiation	Power level	Irradiation duration	Irradiation channel	Irradiated samples
12/08/2020	100 kW	30 min	Center CT	Co, Fe and Au
12/09/2020	20 kW	15 min	Axial profile CT	Ni
02/26/2021	20 kW	15 min	Axial profile CT	19 Au
			8 RSR positions	8 Au
03/29/2021	1 MW	7min 30 s	Center CT	Au
		5 min	PTS	Co, Ni, Al, Fe, Ti

Table. III. List of the irradiations performed in different channels.

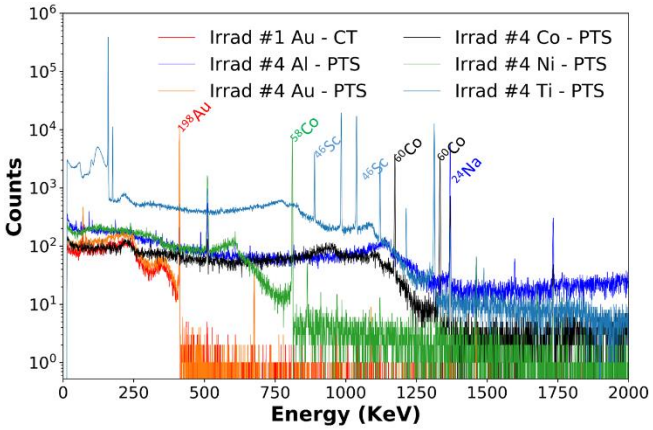

Fig. 2. Experimental gamma-ray spectra of some dosimeters.

4.2. HPGe detector's efficiency

The detector efficiency has been determined through specific measurements with a certified Eu-152 multigamma radioactive source, which allows spreading the energy range from 100 to 1400 keV. The source has a calibrated activity of 43 000 Bq (2σ relative uncertainty of 1.5%) at 12:00:00 (GMT +1) on November 21, 2007. In this calibration, two source–detector configurations were applied, corresponding to source–detector distances of 69.3 and 215.3 mm, which we can refer to as "near" and "far," respectively (see Fig. 11). Fig. 12 presents the gamma-ray spectra for both, "near" and "far" configurations. Once the spectra have been processed, the next step was to carry out an adjustment of the experimental data to obtain the value of the detector's efficiency at the energy E. There are several models to represent the efficiency $R^P(E)$; in our case, we used a logarithmic model:

$$\ln\left(R^P(E)\right) = \sum_{i=0}^{n} a_i [\ln(E)]^i \qquad (4)$$

where a_i are the values of the polynomial coefficients of $R^P(E)$ and E. The uncertainty of the fit is calculated using the associated covariance data:

$$\sigma^2_{\ln\left(R^P(E)\right)} = \sum_i \sum_j \frac{\partial\left[\ln\left(R^P(E)\right)\right]}{\partial a_i} cov\left(a_i, a_j\right) \frac{\partial\left[\ln\left(R^P(E)\right)\right]}{\partial a_j} \quad (5)$$

Different orders (from 2 to 6) of the polynomial fit have been tested, the 4th order polynomial fit has been proven to be the most satisfactory.

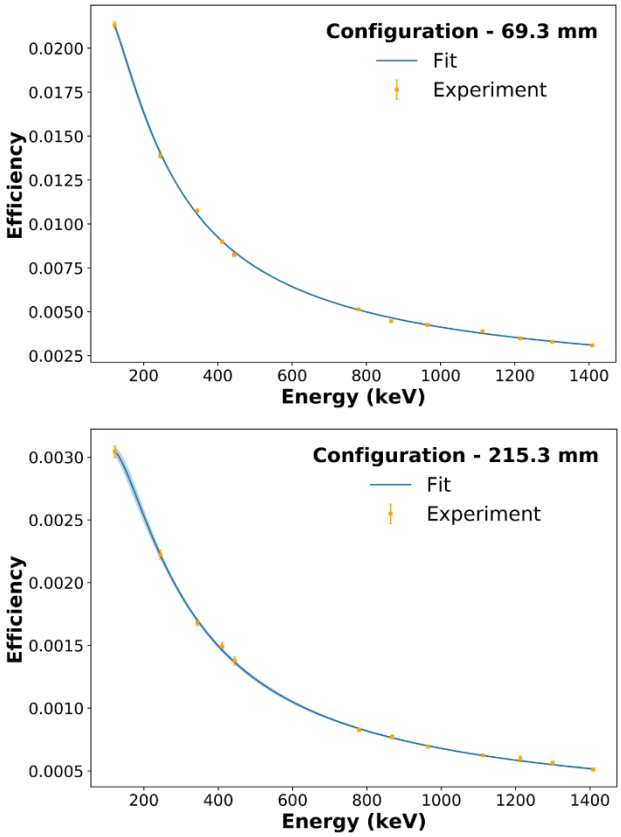

Fig. 3. Yield calibration curves of both, 'near' and 'far', source-detector configurations.

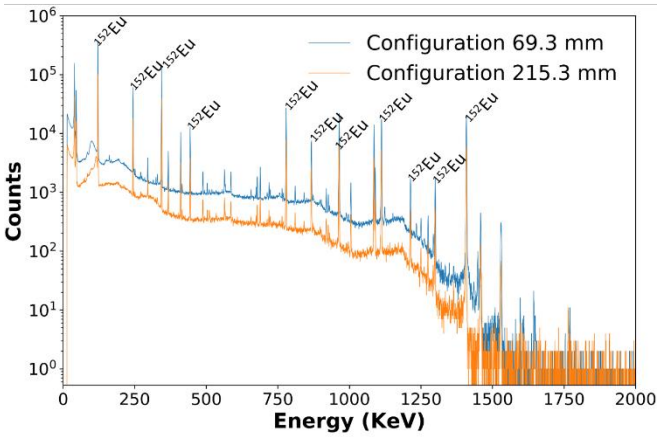

Fig. 4. Gamma-ray spectra of both, 'near' and 'far', source-detector configurations.

4.3. Correction factors

As shown in (3), different correction factors should be applied to accurately quantify the activity at the end of irradiation. These factors were also be applied during the efficiency curve calibration. These coefficients are presented in the following.

1) *Dead-Time Correction*: The dead time is due to the time required for the electronics to process the signals delivered by the detector. The most widely used method for the correction of dead time consists of extending the measurement time by the time

required to analyze the signals. We, therefore, define a real measurement time tr and an active time ta during which the chain of measurement is occupied by the processing of a pulse in the detector. The factor $1 - t_a/t_r$ then corresponds to the percentage of dead time during the measurement. The acquisition software evaluates the dead time in each measurement.

2) Correction of Coincidences $\gamma - \gamma$, $\gamma - X$, and $X - X$ (commonly called "Peak Sum"), or $C\gamma\gamma$: The phenomenon of coincidence comes from the detection of two simultaneous photons emitted in cascade. This phenomenon is more important when the source–detector distance is small (wide solid angle). The corrections can be determined using the Efficiency Transfer for Nuclide Activity (ETNA) measurements software [11], developed by the Henri Becquerel National Laboratory (LNHB). In our case, we applied this correction only for the "near" source–detector configuration. The $C\gamma\gamma$ coefficients, in the case of the "far" configuration, are considered negligible, around 1.001. The results for the coincidence corrections for the "near" configuration are presented in Table IV.
3) *Yield Transfer Factor* T: This factor corrects the dosimeter measurements to take the spatial distribution of the gamma source into account inside it (solid angle, gamma-ray absorption in the dosimeter material). For that reason, the TRIPOLI-4 model of the CNESTEN's HPGe detector was used to carry out photon simulations to evaluate the yield transfer factor. This factor was calculated with the following formula:

$$T(E_0) = \frac{\eta_v(E_0)}{\eta_0(E_0)} \tag{6}$$

where $\eta_v(E_0)$ is the detector's efficiency of a source of energy E_0, resulting from an elementary volume representative of the dosimeter; $\eta_0(E_0)$ is the detector's efficiency of a fictive point source of energy E_0 placed in the same geometric configuration as for the reference calibration. The results of the TRIPOLI-4 simulations are presented in Table IV.

Radionuclide	Energy (keV)	Yield transfer factor T4	σ_{T4}	$C_{\gamma\gamma}$
^{197}Au(n, γ)^{198}Au	411.80	0.9902	0.36%	-
^{58}Ni(n, p)^{58}Co	810.76	0.9980	0.47%	-
^{56}Fe(n, p)^{56}Mn	846.76	0.9911	0.48%	1.0040
	1810.76	0.9941	0.42%	1.0201
^{46}Ti(n, p)^{46}Sc	889.79	0.9966	0.48%	1.0101
	1120.12	0.9976	0.49%	1.0101
^{59}Co(n, γ)^{60}Co	1173.23	0.9863	0.54%	1.0101
	1332.49	1.0053	0.56%	1.0101
^{27}Al(n, α)^{24}Na	1368.63	0.9978	0.57%	1.0101
	2754.05	0.9988	0.53%	1.0101

Table. IV. evaluation of the yield transfer factor by TRIPOLI-4 simulations and correction of coincidences for the "near" configuration by ETNA.

4) *Decay Correction Factor* C_{dec}: This factor is applied to consider the radioactive decay during cooling after irradiation and during measurement. This factor is expressed by:

$$C_{dec} = \frac{\lambda t_m}{e^{-\lambda t_d}(1 - e^{-\lambda t_m})} \tag{7}$$

where λ is the decay constant in s^{-1}, t_m is the acquisition duration (s) and t_d the duration (s) between the end of irradiation and the beginning of acquisition.

4.4. Uncertainty Quantification

The uncertainty on the measured activity is given by propagating the uncertainties of all the parameters in formula (3). By applying the general law of the propagation of uncertainties and by assuming that the variables are independent of each other, the variance of a physical

quantity M, which is a function of other variables, $M = f\,(x_i)$, can be written as:

$$\sigma_M^2 = \sum_{i=1}^{N} \left(\frac{\partial f}{\partial x_i}\right)^2 \sigma_{x_i}^2 \tag{8}$$

The net area uncertainty combines the statistical and the background estimation uncertainties. The spectrometry measurements were performed such as to keep the statistical counting uncertainty below 1%, meaning that the measured number of counts under the total absorption peak is greater than 10^4 counts. Moreover, the uncertainties of the intensities of the photon emissions are given in [9] and are around 0.001%–0.06% depending on the considered nuclide.

The uncertainty of the fitted efficiency curve is evaluated using the associated covariance data [see (5)]. These uncertainties are around 0.9%–1.3% and around 1% for both near and far source-detector configurations, respectively. Furthermore, the uncertainties on the dosimeters' mass and on the irradiation decay and measurement durations are considered negligible and are not taken into account in this study.

The uncertainties on the correction factors are evaluated by applying the uncertainty propagation law. For the decay correction factor, the uncertainty is calculated by the following formula:

$$u^2(C_{dec}) = C_{dec}^2 \left[1 + \frac{1}{\lambda_X} - \frac{t_r}{e^{\lambda_X t_r} - 1}\right]^2 u(\lambda_X)^2 \tag{9}$$

As shown in (9), the uncertainty on the decay correction factor depends on the uncertainty of the constant decay of the considered nuclide, which is around 0.01%–0.1%. As reported in Table IV, the uncertainties on the yield transfer factor are given by statistical uncertainties, given by TRIPOLI-4 simulations, and are within 0.6%. In the end, the overall uncertainty on the specific activity is around 2% (1σ).

5. Results and discussions

5.1. Reaction rates calculation

In this section, we present the comparison between the calculated and measured RRs in the irradiation channels of the TRIGA reactor. Calculations were performed using the new TRIPOLI-4 model of the reactor and JEFF3.1.1 nuclear data library at 300 K. RRs are calculated using the point-wise IRDF-2002, International Reactor Dosimetry File [12].

In simulations, results are expressed as reactions per neutron particle source. To perform an absolute comparison of RRs, the calculated results should be accurately normalized to the reactor power level using the scaling factor defined in [10]. In this study, we will present only the comparison between relative values (see section V-B).

For the RRs in CT and PTS, the simulations were performed in criticality mode using 2.5×10^9 neutrons, leading to a statistical uncertainty on RRs around 1%–2%. For RRs in the RSR facility, simulations were performed using 5×10^9 neutrons, and the statistical uncertainties were around 1%–3%. The dosimeters were modeled explicitly, taking their real dimensions and compositions into account. The irradiation devices were also explicitly modeled inside the irradiation channels of the reactor. In addition to that, the positions of control rods were modeled accurately to be as representative as possible to the irradiation conditions.

5.2. Comparison of normalized RRs

In this study, the measured and calculated specific activities are normalized to be qualitatively compared. Thus, we compare the relative values without taking the reactor power and its uncertainty into account. The measured and calculated values were normalized to the maximum in the case of the CT facility:

$$A_{i,norm}^{CT} = \frac{A_i^{CT}}{A_{max}^{CT}} \tag{10}$$

Also, to the average for PTS and RSR facilities:

$$A_{i,norm}^{RSR,PTS} = \frac{A_i^{RSR,PTS}}{\frac{1}{i_{max}} \sum_i^{i_{max}} A_i^{RSR,PTS}} \tag{11}$$

where A_i are the specific activities at the end of irradiation expressed in Bq.mg^{-1}.

Figs. 13–16 show the comparisons of the normalized measured and calculated values of specific activities. In each graph, the blue area in the middle indicates the active fuel region of a standard FE. The $C/E-1$ relative differences, between calculated normalized specific activities and measured ones, are presented in the following in each graph.

Figs. 13 and 14 refer to the comparison between normalized calculated and measured axial profiles in the CT channel. The profiles are achieved using different gold and nickel dosimeters that were fixed axially in different positions on the irradiation device (see Fig. 3). The simulations were performed by explicitly modeling the dosimeters in the same positions in the irradiation device. The results show a good agreement between the calculated and measured values. For the axial distribution of the ^{197}Au(n, γ)^{198}Au RR, the values of $(C/E-1)$ are around 3% in the active fuel region and around 7% in the reflector area of the FE. In the case of the ^{58}Ni(n, p)^{58}Co RR, the relative differences $(C/E-1)$ are around 2%–10% in the active fuel region and around 20% in the reflector parts of the FE. Further work is required to identify the cause of the discrepancy in the fast flux shape on the bottom part.

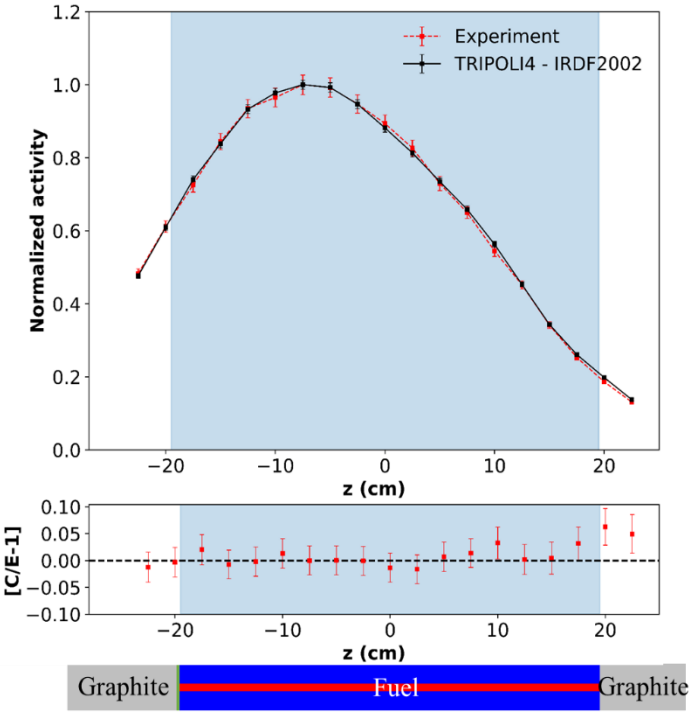

Fig. 5. Measured and calculated axial profile of ^{197}Au(n, γ)^{198}Au RRs in the CT, normalized to the maximal value. The area marked in blue corresponds to the active fuel region of the standard fuel element.

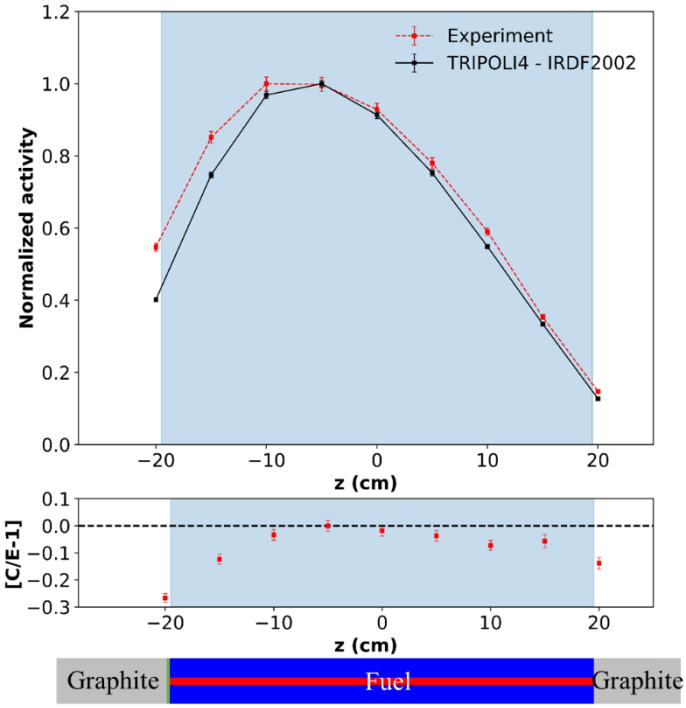

Fig. 6. Measured and calculated axial profile of ^{58}Ni(n, p)^{58}Co RRs in the CT, channel normalized to the maximal value. The area marked in blue corresponds to the active fuel region of the standard fuel element.

The preliminary analysis of the axial gold and nickel RR profiles has shown a slight systematic shift in the axial direction, which was corrected by simulations. This shift may be related to the bad knowledge of the configuration of the bottom-end of the CT. For RSR facility, the RRs were calculated using explicit dosimeters that were modeled inside polyethylene capsules and then positioned in the irradiation channels. Fig. 15 shows a good agreement between the measured and calculated normalized gold RRs in the eight measured positions among the 40 in the RSR facility. The relative differences between the calculated and experimental values are around 1% and 6%. However, the statistical uncertainty in the calculated RRs lies between 1% and 5% (in IC#20).

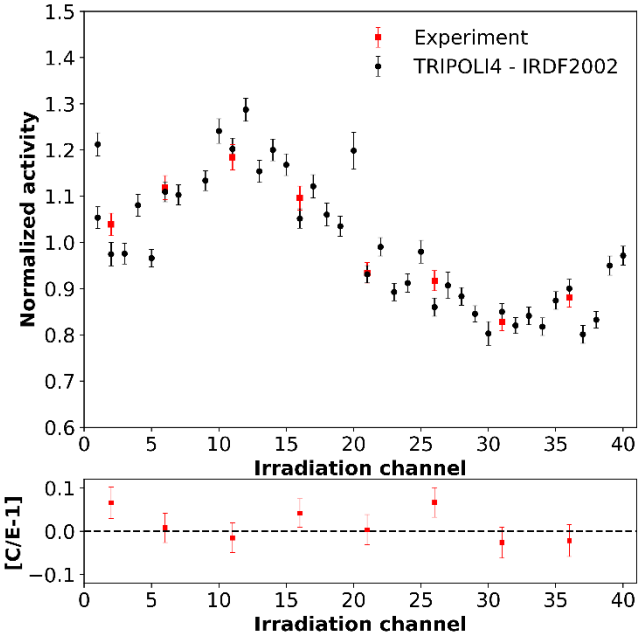

Fig. 7. Measured and calculated ^{197}Au(n, γ)^{198}Au RRs in the RSR irradiation facility normalized to the average value.

The simulations in the PTS facility were performed at z = −28 cm (regarding the core center), which we assume that is in agreement with the measurement position. Fig. 16 displays the calculated and measured RRs for five types of dosimeters: ^{197}Au(n, γ), ^{27}Al(n, α), ^{46}Ti(n, p), ^{58}Ni(n, p), and ^{59}Co(n, γ).

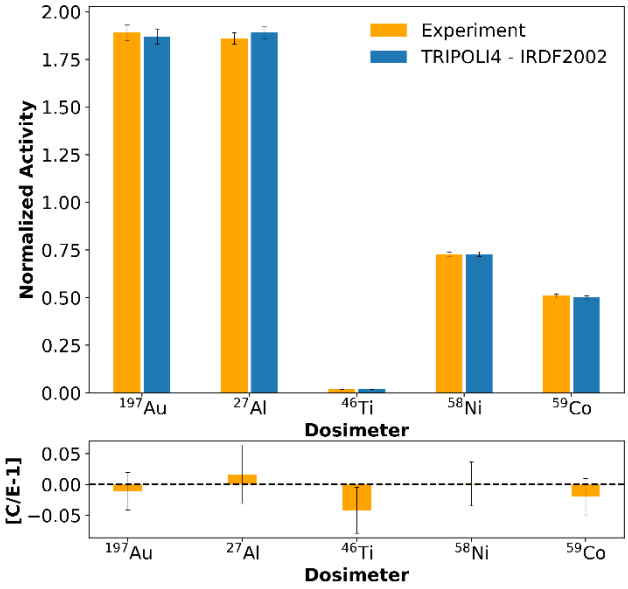

Fig. 8. Measured and calculated RRs for different samples irradiated in the PTS normalized to the average value in the PTS irradiation facility.

As mentioned before, the calculated and measured values were normalized to the average values of all dosimeters irradiated in the PTS. Moreover, a good agreement among the results is shown for all dosimeters irradiated in the PTS. The $C/E-1$ ratios are within 1%–4% (maximum difference for ^{46}Ti dosimeter), which indicates that the TRIPOLI-4 model can accurately reproduce the relative experimental RRs.

6. Conclusion

The study presented in this article aims at demonstrating the capability of the new TRIPOLI-4 model to reproduce the results of the activation measurements that were carried out in the irradiation channels of the CNESTEN's TRIGA reactor. Through comparisons between calculated and measured RRs, we demonstrate that the TRIPOLI-4 model is able to calculate relative RRs consistent with experimental measurements and can be used to design future experiments within the reactor core and the irradiation devices (PTS and RSR) surrounding it.

The absolute measured RRs still need to be processed by considering the irradiation power level during the experiments. In addition, the unfolding of the energy domains of the neutron spectrum is going to be achieved in two positions in the reactor core, in the PTS, and in the core center. Moreover, we are also going to study and take the impact of the burn up into account to the calculated and measured RRs.

As a next step in the measurement analysis, the different sources of uncertainties, more specifically the technological ones and nuclear data uncertainties, are going to be identified and evaluated to estimate their impact on the results.

7. Acknowledgement

The authors would like to thank the members of the MADERE Platform of Instrumentation Sensors and Dosimetry Laboratory (LDCI), French Atomic Energy and Alternative Energies Commission (CEA), Saint-Paul-lez-Durance, France, for providing the dosimeters used in this study and for their valuable technical support on gamma spectrometry measurements.

8. References

[1] X-5 Monte Carlo Team, MCNP—A General Monte Carlo N-Particle Transport Code, Los Alamos Nat. Lab., NM, USA, 2003.

[2] B. E. Bakkari et al., “Monte Carlo modelling of TRIGA research reactor,” Radiat. Phys. Chem., vol. 79, no. 10, pp. 1022–1030, Oct. 2010.

[3] E. Chham et al., “Neutronic and thermal–hydraulic analysis of new irradiation channels inside the Moroccan TRIGA MARK II research reactor core,” Appl. Radiat. Isot., vol. 116, pp. 178–184, Oct. 2016.

[4] H. E. Yaakoubi et al., “Neutronic study of the 2-MW TRIGA MARK-II research reactor by the deterministic codes DRAGON5 & DONJON5,” Appl. Radiat. Isot., vol. 157, Mar. 2020, Art. no. 109026.

[5] Y. Boulaich et al., “Steady-state thermal-hydraulic analysis of the Moroccan TRIGA MARK II reactor by using PARET/ANL and COOLOD-N2 codes,” Nucl. Eng. Des., vol. 241, no. 1, pp. 270–273, Jan. 2011.

[6] E. Brun et al., “TRIPOLI-4®, CEA, EDF and AREVA reference Monte Carlo code,” Ann. Nucl. Energy, vol. 100, no. 82, pp. 151–160, 2015.

[7] A. Santamarina et al., “The JEFF-3.1.1 nuclear data library,” Nuclear Energy Agency Organisation for Economic Co-operation and Development, Paris, France, JEFF Rep. 22, 2009.

[8] J. M. Girard, H. Philibert, S. Testanière, C. Domergue, and D. Beretz, “The MADERE radio-activity measurement platform: Developments for a better addressing to the experimental needs,” in Proc. 1st Int. Conf. Advancements Nucl. Instrum., Meas. Methods Appl., Jun. 2009, pp. 1–8.

[9] Library for Gamma and Alpha Emissions—CEA/LNHB. Accessed: 2021. [Online]. Available: http://www.lnhb.fr/donnees-nucleaires/module-lara/

[10] L. Snoj and M. Ravnik, “Calculation of power density with MCNP in TRIGA reactor,” in Proc. Int. Conf. Nuclear Energy New Europe, Portorož, Slovenia, Sep. 2006, pp. 1–6.

[11] M.-C. Lépy, “Total efficiency calibration for coincidence-summing corrections,” Nucl. Instrum. Methods Phys. Res. A, Accel., Spectrometers, Detectors Associated Equip., vol. 579, no. 1, pp. 284–287, 2007.

[12] O. Bersillon, “International reactor dosimetry file 2002 (IRDF-2002),” Int. At. Energy Agency, Vienna, Austria, Tech. Rep., 452, 2006.